Antenna Characterization from a Small Number of Far-Field Measurements via Reduced-Order Models

N. Mezieres, M. Mattes, Benjamin Fuchs

This article has been accepted for publication in a future issue of this journal, but has not been fully edited. Content may change prior to final publication. Citation information: DOI 10.1109/TAP.2021.3118711, IEEE Transactions on Antennas and Propagation

Antenna Characterization from a Small Number of Far-Field Measurements via Reduced-Order Models

Nicolas Mézières, Michael Mattes and Benjamin Fuchs, *Senior Member, IEEE*

***Abstract*—The determination of a small number of samples to characterize the antenna far field with a controlled accuracy is addressed. The radiation operator that maps the equivalent currents to the far field is built from the outer dimensions of the antenna under test and is discretized into the so-called radiation matrix using the methods of moments. This matrix is approximated up to the measurement accuracy by truncating its singular value decomposition accordingly. This operation enables to construct numerically a reduced basis of the radiated fields. The dimension of this basis and consequently the number of field samples is shown to be determined by the area of the equivalent current convex surface, in agreement with the fundamental works on the minimum non-redundant samplings. The influence of the field sampling strategy and noise on the far-field pattern reconstruction are investigated in order to determine a realistic small number of field samples. Finally, the characterization of two radiating structures from the so-derived reduced number of samples validates experimentally the proposed approach and demonstrates its practical relevance.**

***Index Terms*—Antenna measurements, antenna radiation pattern, method of moments, reduced order systems.**

I. Introduction

FAST antenna characterization is a very active field of present-day research because of its important industrial relevance. In this regard, a lot of different techniques have been developed through the years [1]. The characterization of antennas is a time consuming but necessary task to validate the design and the manufacturing of radiating structures. The most efficient way to speed up antenna characterization is to reduce the number of field samples and therefore the field acquisition duration. The goal of this paper is precisely to develop a systematic method to reduce the number of samples to characterize the far-field pattern radiated by a given antenna with a controlled accuracy.

The field radiated by antennas of finite sizes can be expanded using truncated series [2], [3]. The choice of this expansion depends on *a priori* information about the antenna (e.g. shape, maximum electrical length) and has an impact on the number of field samples for its characterization. Nowadays, the Spherical Wave (SW) expansion is a standard technique for spherical near- and far-field antenna 3D measurements. In addition to being solutions to Maxwell's equations, SW form an orthogonal basis of functions defined over the sphere. The number of SW in the expansion depends on the maximum electrical dimension of the Antenna Under Test (AUT) [2]. The number of field samples to identify these SW expansion coefficients is often referred to as Nyquist sampling, understood as a generalization to the classical theorem for Fourier series.

A recent line of research has leveraged the sparse SW expansion of the field radiated by antennas to reduce the number of field samples [4]–[7]. This strategy enables to approximately halve the required number of field samples as compared to the so-called Nyquist sampling. However, this sparse SW expansion only provides an approximated interpolation of the field radiated by the AUT.

Other analytical expansions have been proposed and successfully validated by Prof. Bucci *et al.* [3], [8]–[10]. These function bases better exploit the true shape of the AUT by enclosing it in a convex surface with an axial symmetry. More importantly and despite the geometrical limitations imposed by the use of analytical basis functions, this fundamental and pioneer work ensures the minimal number of samples.

The analytical approaches, either the SW expansion [2] or the minimum non-redundant sampling [10], rely on limited spatial-bandwidth assumption to provide an optimal sampling rate. This paper aims to further harness the geometry of the AUT as well as the one of the measurement surface with a controlled accuracy level on the reconstruction.

Numerical approaches have been used in recent works to combine strong *a priori* information and numerical simulations of the AUT in order to expedite its characterization. Full-wave electromagnetic simulations of the AUT structure can be used to build a compressed [11], [12] or overcomplete [13] representation of the radiated fields, enabling the reconstruction of the AUT radiation pattern from a small number of field samples. Both strategies lead to fast antenna testings when strong priors about the AUT are available.

The construction of a reduced-order model is achieved by a Singular Value Decomposition (SVD). The SVD has been previously used successfully for solving inverse problems related to antenna measurement and diagnostic problems [14], [15] as well as to speed up the analysis of large antennas [16]. However, the construction and use of reduced-order models to speed up antenna characterization is relatively new. Initially proposed to efficiently characterize the radar cross section of targets [17], this approach has been recently applied to bring down the number of samples for the characterization of

Manuscript received xx, 2021; revised xx, xx.

This work was carried out in the frame of a CNES and LNE grant and is supported in part by the European Union through the European Regional Development Fund (ERDF), and by the french region of Brittany, Ministry of Higher Education and Research, Rennes Métropole and Conseil Départemental 35, through the CPER Project SOPHIE / STIC & Ondes.

N. Mézières is with IETR, CNES and LNE (e-mail: nicolas.mezieres@univ-rennes1.fr). M. Mattes with the Technical University of Denmark, 2800 Kongens Lyngby, Denmark. B. Fuchs is with the IETR, UMR CNRS 6164, Rennes, France.

Digital Object Identifier

antennas [18]. The proposed reduced-order model approach requires to know the AUT outer dimensions and the measurement surface geometry.

This paper describes a procedure to build the reduced antenna characterization model with a controlled accuracy. The derivation of a reduced number of field samples for a given AUT is also detailed, compared to existing works, and experimentally validated. The proposed methodology can be summarized as follows:

1) The AUT, given its external dimensions and position in the measurement coordinate system, is enclosed in a surface mesh.
2) The radiation matrix is computed for the given sampling positions.
3) A truncated singular value decomposition is performed to provide a reduced-order model of the antenna characterization problem.
4) The measured field is expanded into the basis given by the model and this expansion is used to interpolate the field where needed.

The paper is organized as follows: the construction and discretization of the radiation operator (steps 1 and 2) involved in the antenna characterization problem is detailed in Section II. The operations to build the reduced-order antenna characterization model with a controlled accuracy from the radiation matrix (step 3) are described in Section III. A reduced number of field samples is discussed in Section IV (step 4). Its link to the area of the equivalent surface around the AUT is given. The influence of the type of sampling and the noise is investigated. Experimental validations of our antenna far-field characterization procedure from a small number of samples are shown. Finally, in Section V, we provide some conclusions.

II. Radiation Operator of the Antenna Characterization

In the following sub-sections are described the construction and discretization of the radiation operator that maps the equivalent currents on the surface enclosing the AUT to the radiated field.

A. Surface Equivalence Principle

In electromagnetics, the fields $(\mathbf{E}, \mathbf{H})$ radiated by a set of finite sources $(\mathbf{J}, \mathbf{M})$ can be described by equivalent surface electric and magnetic current distributions that represent the tangential magnetic and electric fields, respectively [19]. This equivalence principle, also known as Huygens' principle, means that the field radiated by the AUT enclosed by a surface Σ can be represented by equivalent surface currents $(\mathbf{J}_{eq}, \mathbf{M}_{eq})$ on it, as depicted in Fig. 1.

There are different variants of the surface equivalence principle depending on the constraints imposed on the internal fields $\mathbf{E}'$ and $\mathbf{H}'$ in Fig. 1. Love's formulation, also known as zero internal fields constraint, for which $\mathbf{E}' \equiv 0 \equiv \mathbf{H}'$, has been shown to provide realistic current distributions [20], [21]. Besides, note that only one type of equivalent current ($\mathbf{J}_{eq}$ or $\mathbf{M}_{eq}$) can suffice provided that the volume V is filled with either a perfect magnetic or electric conductor, respectively.

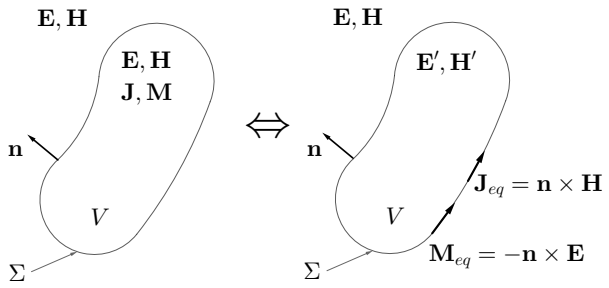

Fig. 1. Surface equivalence principle : the original problem (left) can be replaced by an equivalent one (right). The electromagnetic field $(\mathbf{E}, \mathbf{H})$ outside a volume V enclosed by a surface Σ containing all the sources is radiated by equivalent current distributions $\mathbf{J}_{eq} = \mathbf{n} \times \mathbf{H}, \mathbf{M}_{eq} = \mathbf{E} \times \mathbf{n}$ over Σ.

In this paper, the goal is to interpolate at best the electric far field radiated by the AUT enclosed by Σ. Therefore, we leave the internal fields $\mathbf{E}'$ and $\mathbf{H}'$ unconstrained and use both types of equivalent currents, as suggested in [22], [23].

B. Integral Equations

1) Boundary integral equation: The electric field radiated by the equivalent surface currents $(\mathbf{J}_{eq}, \mathbf{M}_{eq})$ on Σ into a source-free region, characterized by its permeability μ, its permittivity ε and employing the Lorenz gauge, is given by

$$\begin{aligned}\mathbf{E}(\mathbf{r}) = j\omega\mu \int_{\Sigma} g(\mathbf{r}, \mathbf{r}')\mathbf{J}_{eq}(\mathbf{r}')d\sigma' \\ - \frac{1}{j\omega\varepsilon} \int_{\Sigma} \mathbf{grad}_{\mathbf{r}} g(\mathbf{r}, \mathbf{r}')\text{div } \mathbf{J}_{eq}(\mathbf{r}')d\sigma' \\ - \int_{\Sigma} \mathbf{rot}_{\mathbf{r}}\big(g(\mathbf{r}, \mathbf{r}')\mathbf{M}_{eq}(\mathbf{r}')\big)d\sigma'\end{aligned} \tag{1}$$

where ω is the angular frequency and g the scalar free-space Green function, $g(\mathbf{r}, \mathbf{r}') = \frac{e^{-jk\|\mathbf{r}-\mathbf{r}'\|}}{4\pi\|\mathbf{r}-\mathbf{r}'\|}$. The vector $\mathbf{r}$ is the observation point and $\mathbf{r}'$ is the one used for the integration over Σ. The time convention $e^{j\omega t}$ has been used. The notations $\mathbf{grad}_{\mathbf{r}}$ and $\mathbf{rot}_{\mathbf{r}}$ mean that these operators are applied with respect to the observation position $\mathbf{r}$ only. Equation (1) is valid for all observation points $\mathbf{r}$ outside V.

2) Boundary element method: The equivalent current distributions $(\mathbf{J}_{eq}, \mathbf{M}_{eq})$ that are tangential to the surface Σ and radiate the same field as the sources $(\mathbf{J}, \mathbf{M})$ contained in the volume V are assumed to be expanded into a set of known basis functions $\mathbf{f}_k, k = 1, \ldots, K$ defined over Σ, yielding

$$\begin{aligned}\mathbf{J}_{eq}(\mathbf{r}') = \sum_{k=1}^{K} \mathrm{j}_k \mathbf{f}_k(\mathbf{r}'), \\ \mathbf{M}_{eq}(\mathbf{r}') = \eta \sum_{k=1}^{K} \mathrm{m}_k \mathbf{f}_k(\mathbf{r}').\end{aligned} \tag{2}$$

where j_k and m_k are the complex expansion coefficients. Note that the equivalent magnetic current is multiplied by the wave impedance η so that both currents $(\mathbf{J}_{eq}, \mathbf{M}_{eq})$ have the same order of magnitude, as often advocated [21].

The current expansions (2) transform the surface integrals (1) into a weighted sum of integrals of the known basis

This article has been accepted for publication in a future issue of this journal, but has not been fully edited. Content may change prior to final publication. Citation information: DOI 10.1109/TAP.2021.3118711, IEEE Transactions on Antennas and Propagation

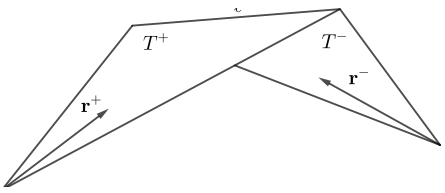

Fig. 2. Illustration of the support of a RWG basis function : ℓ is the length of the common edge, $T^{\pm}$ denote the triangles and $\mathbf{r}^{\pm}$ the position vectors from the opposite vertices. The current flows from T^+ to T^-.

functions. Thus, the contribution of the basis function $\mathbf{f}_k$ to the radiated field, denoted $\mathbf{E}_k$, is given by :

$$\begin{aligned}\mathbf{E}_k(\mathbf{r}) = \mathrm{j}_k \Bigg[& j\omega\mu \int_\Sigma g(\mathbf{r},\mathbf{r}')\mathbf{f}_k(\mathbf{r}')d\sigma' \\ & -\frac{1}{j\omega\varepsilon}\int_\Sigma \mathbf{grad}_{\mathbf{r}} g(\mathbf{r},\mathbf{r}')\mathrm{div}\ \mathbf{f}_k(\mathbf{r}')d\sigma' \Bigg] \\ & -\eta \mathrm{m}_k \int_\Sigma \mathbf{rot}_{\mathbf{r}}\big(g(\mathbf{r},\mathbf{r}')\mathbf{f}_k(\mathbf{r}')\big)d\sigma'.\end{aligned} \tag{3}$$

By doing so, the original integral equation is approximated by an easier to solve coefficient identification problem, where the unknowns are the weights j_k and m_k.

C. Construction of the Radiation Operator

The boundary element method can be implemented in various manners. Our choices regarding the basis functions $\mathbf{f}_k$, the numerical integration rule and the matrix construction are now given.

1) RWG functions: The surface Σ containing the equivalent currents is approximated by triangles. We consider Rao-Wilton-Glisson (RWG) [24] basis functions. This choice is widely spread for its ease of computation while ensuring continuous normal fluxes across the common edge of two adjacent triangles. Each couple of adjacent triangles, sharing an edge, defines a basis function, which is computed as follows following the notations given in Fig. 2

$$\mathbf{f}(\mathbf{r}) = \begin{cases} \frac{\ell}{2A^+}\mathbf{r}^+ & \text{if } \mathbf{r}\in T^+, \\ -\frac{\ell}{2A^-}\mathbf{r}^- & \text{if } \mathbf{r}\in T^-, \\ 0 & \text{otherwise.}\end{cases} \tag{4}$$

where $A^{\pm}$ are the areas of the triangles $T^{\pm}$, respectively.

2) Numerical integration: For a given observation position $\mathbf{r}$ and using the Gauss-Legendre quadrature rule, each integral term in (3) is evaluated. The 9-points version for a triangular integration domain of the quadrature rule is used [25]. In our measurement context, the observation point $\mathbf{r}$ is always far enough from the equivalent surface Σ and thus from $\mathbf{r}'$. Consequently, each term of (3) is well-defined as singularities are avoided. Hence, the integrands are smooth enough for the Gauss-Legendre quadrature to be accurate.

3) Matrix formulation: The equation (3) is valid for any observation point $\mathbf{r}$ in the external region (outside V). Let us consider a set $\mathbf{r}_m$ of M observation points. Equation (1) can be approximated and formulated in Cartesian coordinates as follows

$$\begin{bmatrix}\mathbf{E}_x \\ \mathbf{E}_y \\ \mathbf{E}_z\end{bmatrix} = \begin{bmatrix}\mathbf{A}_{J,x} & \eta\mathbf{A}_{M,x} \\ \mathbf{A}_{J,y} & \eta\mathbf{A}_{M,y} \\ \mathbf{A}_{J,z} & \eta\mathbf{A}_{M,z}\end{bmatrix}\begin{bmatrix}\mathbf{j} \\ \mathbf{m}\end{bmatrix} \tag{5}$$

where $\mathbf{E}_x$ contains the x-component of $\mathbf{E}$ at the observation positions $\mathbf{r}_m$, $\mathbf{A}_{J,x}$ the x-component of the electric current distribution in the equation (3) for each basis functions $\mathbf{f}_k$, $\mathbf{A}_{M,x}$ is the same for the magnetic current distribution. The other components in y and z are defined similarly. Finally, the vectors $\mathbf{j}$ and $\mathbf{m}$ gather all the coefficients of the equivalent currents, j_k and m_k, to be determined. Systems of equations similar to (5) can be easily derived when other vector field representations are used.

In the sequel, the system (5) is denoted by $\mathbf{y} = \mathbf{A}\mathbf{x}$, where the vector $\mathbf{y}$ contains the measured field, $\mathbf{A}$ is the discretized radiation operator and $\mathbf{x}$ the equivalent currents.

III. Reduced Antenna Characterization Model

In this part, the steps to construct the reduced antenna characterization model from the radiation matrix are described.

A. Truncated Singular Value Decomposition

The radiation matrix $\mathbf{A}$ is, in general, not of full rank. Many sets of currents $\mathbf{x}$ lead to the same radiated field $\mathbf{y}$. Therefore, the matrix $\mathbf{A}$ can be approximated by $\mathbf{A}_{\mathrm{T}}$, for which only the T largest singular values are kept:

$$\mathbf{A} \approx \mathbf{A}_{\mathrm{T}} = \mathbf{U}\mathbf{S}_{\mathrm{T}}\mathbf{V}^H \tag{6}$$

where $\mathbf{V}^H$ is the conjugate transpose (also called Hermitian transpose) of $\mathbf{V}$. The columns of $\mathbf{V}$ form an orthonormal basis of the equivalent current distributions over the equivalent surface Σ while the columns of $\mathbf{U}$ are the associate orthonormal modes of the fields that can be radiated by the enclosed AUT. The diagonal matrix $\mathbf{S}_{\mathrm{T}}$ contains the first T singular values $\sigma_1 \geq \sigma_2 \geq \cdots \geq \sigma_{\mathrm{T}}$. The field $\mathbf{y}$ radiated by the AUT is expanded into the first T columns of $\mathbf{U}$ as follows

$$\mathbf{y} \approx \mathbf{U}_{\mathrm{T}}\boldsymbol{\nu} \tag{7}$$

where $\boldsymbol{\nu}$ is the new unknown vector of length T. The quality of the approximation (7) is determined by the truncation index T.

B. Choice of the Truncation Index

The choice of the truncation index T, and consequently the size of the radiated field basis $\mathbf{U}_{\mathrm{T}}$, is critical, so to be able to reconstruct properly the radiated field in $\mathbf{y}$ [26]. For the antenna characterization problem, this index is connected to the noise floor level of the measurement system.

Let us consider a reference field measurement $\mathbf{y}$ and its estimation $\widetilde{\mathbf{y}}$. For a measurement noise floor of R dB, we consider that $\mathbf{y}$ and $\widetilde{\mathbf{y}}$ are identical when the average difference between each sample of these two fields is smaller than R dB. This can be translated into $\|\mathbf{y}-\widetilde{\mathbf{y}}\| \leq \delta$ with $\delta = \sqrt{M}\|\mathbf{y}\|_\infty 10^{R/20}$, where M is the size of the measurement vector $\mathbf{y}$ or $\widetilde{\mathbf{y}}$.[1]

The radiation matrix $\mathbf{A}$ is well approximated by $\mathbf{A}_{\mathrm{T}}$ provided that the following inequality holds true for all possible sets of equivalent currents $\mathbf{x}$

$$\|\mathbf{A}\mathbf{x} - \mathbf{A}_{\mathrm{T}}\mathbf{x}\| \leq \delta. \tag{8}$$

[1]The notation $\|\cdot\|$ denotes the Euclidean norm, also often written $\|\cdot\|_2$, $\|\cdot\|_1$ is the sum of magnitudes and $\|\mathbf{y}\|_\infty$ the maximum magnitude among the components of $\mathbf{y}$.

This article has been accepted for publication in a future issue of this journal, but has not been fully edited. Content may change prior to final publication. Citation information: DOI 10.1109/TAP.2021.3118711, IEEE Transactions on Antennas and Propagation

The left hand side of (8) is bounded by $\|\mathbf{A} - \mathbf{A}_{\mathrm{T}}\|\|\mathbf{x}\| = \sigma_{\mathrm{T}+1}\|\mathbf{x}\|$ since we use a normed algebra and $\|\mathbf{B}\|$ is equal to the largest singular value of the matrix $\mathbf{B}$. Using the same properties, $\|\mathbf{y}\| = \|\mathbf{A}\mathbf{x}\|$ leads to $\|\mathbf{y}\| \leq \|\mathbf{x}\|\sigma_1$. By noticing that $\|\mathbf{y}\| \leq \sqrt{M}\|\mathbf{y}\|_\infty$, we can write

$$\frac{\sigma_{T+1}}{\sigma_1} \leq 10^{R/20}. \tag{9}$$

Note that the criterion (9) is not rigorously equivalent to (8). However, its validity is numerically checked in the next section.

C. Numerical Validation of the Truncation Index

1) Methodology: Let us consider the reference radiated field $\mathbf{y}$ and its estimation $\widetilde{\mathbf{y}}$ computed from the truncated radiation matrix $\mathbf{A}_{\mathrm{T}}$, both of size M. The Equivalence Noise Level (ENL) provides a convenient metric to compare these two radiation patterns and is defined by

$$\mathrm{ENL}(\mathbf{y}, \widetilde{\mathbf{y}}) = 20\log_{10}\left(\frac{\|\mathbf{y} - \widetilde{\mathbf{y}}\|_1}{M\|\mathbf{y}\|_\infty}\right). \tag{10}$$

The ENL is a mean error that is normalized with respect to the maximum of the reference field. Adding a white noise of R dB to $\mathbf{y}$ to generate $\widetilde{\mathbf{y}}$ yields $\mathrm{ENL}(\mathbf{y}, \widetilde{\mathbf{y}}) \approx R + 2$ dB.

The truncation index T is chosen such that $\mathrm{ENL}(\mathbf{y}, \widetilde{\mathbf{y}}) \leq R$ for any field $\mathbf{y}$ radiated by an AUT inside the equivalent current surface Σ.

2) Validation: Let us consider the case where the AUT is enclosed by a spherical equivalent surface Σ. Any field radiated by the AUT can be expanded into SW. These SW are denoted $\mathbf{F}_{smn}$ where s is the propagating mode, $s \in \{1, 2\}$, m the order and n the degree, $|m| \leq n$, $1 \leq n \leq N$. Indexes m, n are also integers and N is the truncation order, given by [2]

$$N = \lfloor ka \rfloor + n_1 \tag{11}$$

where k is the wavenumber, a the radius of the smallest sphere enclosing the sources, $\lfloor \cdot \rfloor$ is the integer part function and n_1 a positive integer. A safety margin of $n_1 = 10$ is a widely spread choice as it is valid for most antennas, as advocated by [27]. Other choice of margins have been proposed, such as $n_1 = \beta(ka)^{1/3}$ where β if a real constant for large antennas [28].

For numerical validation purposes, we consider a spherical equivalent surface Σ of radius $a = 2\lambda$, $\lambda = 0.1$ m and a noise floor $R = -50$ dB. The singular value distribution of the resulting radiation matrix is shown in Fig. 3. The truncation index T given by the criterion is also reported and corresponds to the number of SW for $n_1 = 7$, or $N = 19$. The radiation matrix $\mathbf{A}$ is well approximated by $\mathbf{A}_{\mathrm{T}}$ provided that any SW up to $N = 19$, $\mathbf{F}_{s,19,19}$, can be reconstructed with an ENL below R dB.

The SW of highest degree and order, $\mathbf{F}_{s,19,19}$, is the hardest to reconstruct since it exhibits the fastest variations with respect to both directions θ and φ. The results of the reconstruction of several SW are shown in Fig. 4. The truncation index T for a noise floor $R = -50$ dB always leads to an ENL lower than R for all tested SW, validating numerically the proposed criterion (9).

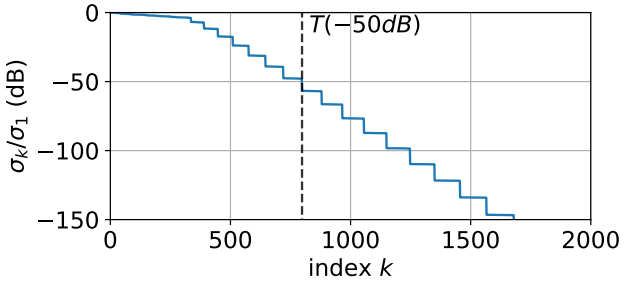

Fig. 3. Normalized singular value distribution of the far-field radiation matrix of a sphere of radius $2\lambda = 0.2$ m. Truncation index T for $R = -50$ dB corresponds to the number of SW in the expansion for $N = 19$. The step widths correspond to the number of SW for each degree n. A similar pattern can also be found in [22].

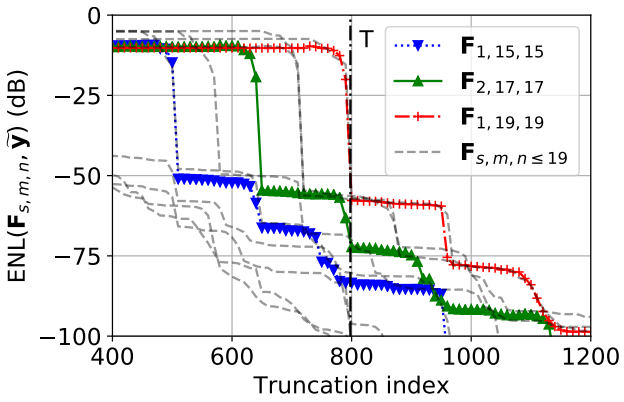

Fig. 4. ENL between the SW, $\mathbf{F}_{smn}$, and $\widetilde{\mathbf{y}}$, its estimation from the truncated radiation matrix $\mathbf{A}_{\mathrm{T}}$. The truncation index $\mathrm{T} = 798$ ensures a proper reconstruction of all SW up to $N = 19$. Unmarked dotted curves show the reconstruction performances of other SW for $n \leq 19$.

D. Singular Values and Equivalent Surface Area

The truncation index T of the singular values is determined by the low-pass behavior of their distribution. Previous analytical works on antenna characterization relying on the radiated field expansion on analytical basis functions have determined that the number of coefficients to retrieve is linked to the area of some canonical convex surface enclosing the sources. More specifically, in the case of spherical near-field measurement as detailed in [2], the truncation order N given in (11) leads to a number of spherical coefficients nearly proportional to $4\pi a^2$, the area of the minimal sphere enclosing the antenna. The work of Prof. Bucci *et al.* [10] provides an explicit relation between the number of so-called degrees-of-freedom of the radiated field for surfaces Σ with some symmetry properties, $N_{deg} = \mathcal{A}(\Sigma)/(\lambda/2)^2$, where $\mathcal{A}(\Sigma)$ is the area of Σ.

It has been numerically checked that two equivalent convex surfaces of same area, no matter their shape, exhibit the same low-pass behavior of their singular value distribution, as illustrated in Fig. 5. It implies that the complexity of the reduced-order model and consequently the number of unknowns in our characterization problem is given by the area of the equivalent convex surface Σ.

This article has been accepted for publication in a future issue of this journal, but has not been fully edited. Content may change prior to final publication. Citation information: DOI 10.1109/TAP.2021.3118711, IEEE Transactions on Antennas and Propagation

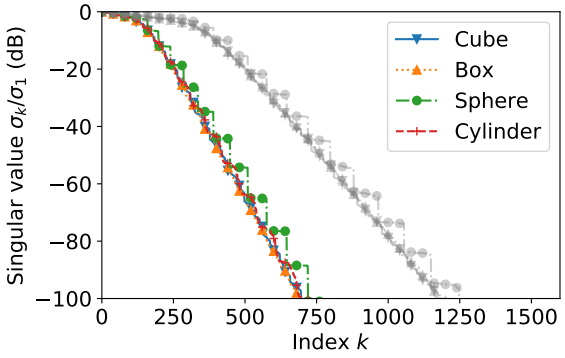

Fig. 5. Normalized singular value distributions for two sets of equivalent surfaces having the same area. The light grey curves correspond to surfaces whose area is twice larger than the colored ones.

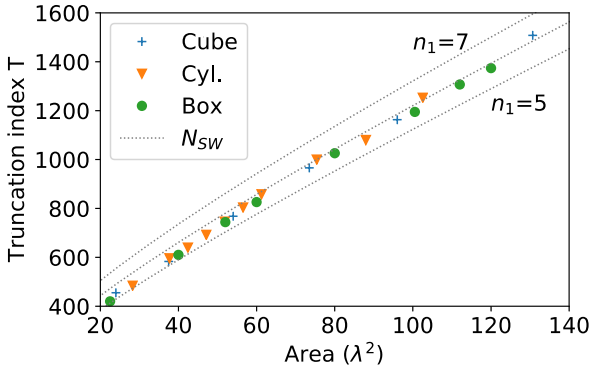

Fig. 6. Truncation index T as a function the surface Σ area enclosing the AUT for various shapes and a noise floor $R = -50$ dB. Three different margins for the number of SW, N_{SW}, $n_1 = 5, 6, 7$, are shown. Note that a cube of side length 4λ has an area of 96 λ^2.

E. Singular Values and Sampling Distributions

A sampling is defined by its size and its distribution over the measurement surface. We can consider the following spherical samplings; Fibonacci's sampling [7], one of the most evenly distributed sampling on the sphere, the *igloo* sampling [6], close to being uniform while providing an easy scan for positioning systems available at IETR. We might also cite the random sampling, where the points are chosen randomly over the sphere, and the equiangular or constant angular step sampling, which is commonly used in spherical near-field measurements [2], or the spiral sampling [29], [30]. Evenly distributed samplings, such as Fibonacci or *igloo*, have been observed to provide very similar singular values distributions, their overall behaviour is as depicted in Fig. 5. The number of field samples has a negligible effect on the singular value distribution as long as it is larger than the number of basis functions. Based on these observations, the validations example are led on evenly distributed samplings on the measurement sphere with more field samples than basis functions.

F. Conclusion

The construction of the reduced antenna characterization model has been detailed, the method to determine the number of basis functions (also called characteristic modes) to represent the far field has been discussed and validated. The order of the antenna characterization model T was shown to be linked to the area of the AUT equivalent surface over the squared half wavelength. This result is in agreement with previous analytical derivations, also known as degrees-of-freedom of radiated fields [3], [9], [10].

IV. Number of Field Samples

The steps to derive the number of field samples from the reduced antenna characterization model are described, validated numerically and experimentally.

A. From the Number of Spherical Waves to the Model Order

The main and remarkable result is that the order T, the truncation index of the reduced antenna characterization model, depends only on the area of the surface Σ whatever its convex shape. Since the number of SW, N_{SW}, is known for a given sphere radius, we can derive the following formula

$$\text{T} = \frac{\mathcal{A}(\Sigma)}{\mathcal{A}(S)} N_{\text{SW}}. \tag{12}$$

where $\mathcal{A}(S)$ is the area of the surface of the minimal sphere. The order of the antenna characterization model is deduced only from the area of the equivalent surface Σ and the maximum dimension of the AUT. An illustration of this statement is shown in Fig. 6, investigated boxes (parallelepipeds) and cylinders have very different aspects ratios.

B. From the Truncation Index to the Number of Samples

The truncation index can be estimated from simple geometrical considerations thanks to (12). The number of field samples from this truncation index T has to be determined to complete our antenna characterization problem. Since noisy measurements and truncation errors are unavoidable and impact the number of required field samples, this leads to considering oversampling factors, as in [10] for example.

1) Methodology: The field $\mathbf{y}$ radiated by the AUT can be expanded using the reduced basis as follows:

$$\mathbf{y} = \sum_{k=1,\dots,\text{T}} \boldsymbol{\nu}_k \mathbf{u}_k + \mathbf{n} \tag{13}$$

where the vector $\mathbf{n}$ stands for the part that is unexplained by the reduced order model, i.e. the measurement noise and the truncation error.

Our goal is to determine the unknown vector $\boldsymbol{\nu}$ of length T from a small number of samples. As in Section III-C, we aim at reconstructing each of the characteristic modes $\mathbf{u}_k, k = 1, \dots, \text{T}$. The modes are known at M_S sampling positions and an additive Gaussian white noise is added to account for measurement uncertainties, leading to the following equation

$$\boldsymbol{\nu}^{(s)} = \arg\min_{\boldsymbol{\nu}} \|\mathbf{y}_k^{(s)} - \mathbf{U}_{\text{T}}^{(s)} \boldsymbol{\nu}\| \tag{14}$$

where $\mathbf{y}_k = \mathbf{u}_k + \mathbf{n}$ for each tested column k and the superscript (s) denotes the subsample of size M_S. The noise magnitude, the mean of $|\mathbf{n}|$, is chosen to be the noise floor R used to derive the truncation index T.

This article has been accepted for publication in a future issue of this journal, but has not been fully edited. Content may change prior to final publication. Citation information: DOI 10.1109/TAP.2021.3118711, IEEE Transactions on Antennas and Propagation

To assess the quality of the reconstruction and thereby the choice of the number of samples M_S, we compute the mean of the reconstruction metrics $\mathrm{ENL}(\mathbf{u}_k, \widetilde{\mathbf{u}}_k)$ for all k where $\widetilde{\mathbf{u}}_k$ is the estimated characteristic mode computed solving (14). As in Section III-C, the reconstruction is said successful when the mean ENL reaches the noise floor R dB.

2) Results: The measurement ratio M_S/T, where M_S is the size of the field sample, is used as a metric to quantify the required number of field samples. The reduced-order model is applied using four sampling strategies (Fibonacci, igloo, random and equiangular) and a spherical equivalent current surface Σ of radius 2λ. The random sampling results are obtained from an average over 20 trials.

As shown in Fig. 7(a), having evenly distributed points is crucial to minimize the number of field samples as the Fibonacci and *igloo* sampling are clearly the first ones to reach the noise floor R, at a measurement ratio ≈ 1.17. This so-called oversampling factor corresponds to the intersection point of the curves with the horizontal line located at the noise floor R. In addition, this factor is rather stable with respect to the measurement noise floor R dB for practically relevant values, as shown by the grey curves in Fig. 7(a). It implies that the number of field samples M_s and the truncation index T increase similarly when the noise floor level R decreases. From these observations, we only consider the *igloo* sampling in the sequel as it is the one applied in our anechoic chambers, while keeping in mind that Fibonacci or spiral samplings behave similarly.

The influence of the equivalent surface shape Σ on the measurement ratio has also been investigated. The results, shown in Fig. 7(b), demonstrate that a measurement ratio of 1.25 is sufficient for all investigated shapes and by extension most antenna geometries.

3) Number of samples: From the previous studies and results, it follows that the number of samples can be set to

$$M_S = \chi \mathrm{T} \tag{15}$$

where T can be estimated from (12) and χ is an oversampling factor, following the notation introduced by Bucci *et al.* [10]. According to our conclusions, an oversampling factor of $\chi = 1.25$ allows a safe characterization in all antenna characterization problems (antenna shape and measurement noise floor).

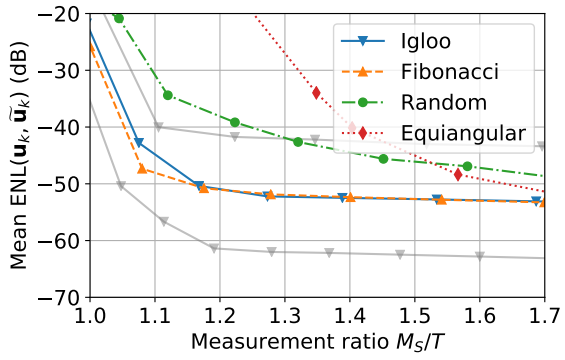

(a)

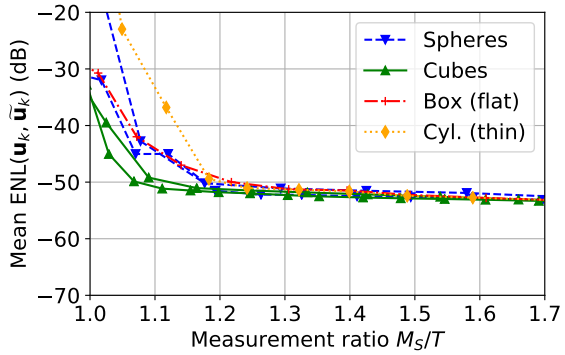

(b)

Fig. 7. Mean ENL reconstructions of the radiated modes for a noise floor $R = -50$ dB. (a) Comparison between sampling strategies : the grey curves are obtained for $R = -40$ and -60 dB with an *igloo* sampling. (b) Comparison of various shapes using an *igloo* sampling.

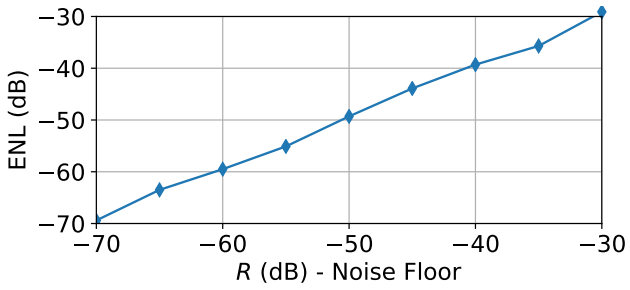

Fig. 8. Mean ENL reconstruction over 50 trials from a noisy sample using the reduced order model of an analytical E-plane horn with sampling ratio ≈ 1.25.

C. Numerical Validation for Various Noise Levels

A first validation is led on an analytical example, an E-plane horn in far field at 20 GHz [31]. The aperture is $1\lambda \times 2\lambda$, located on the plane $z = 0$ and the ridge length is 3λ. It is enclosed in a box of size $1.3\lambda \times 2.3\lambda \times 3.6\lambda$. The radiation matrix is computed on a dense far-field igloo sampling over the hemisphere. For different noise floors R, the reduced-order model is derived and sampling points are selected on a coarser igloo so the sampling ratio is ≈ 1.25. White noise is added such that it corresponds to the noise floor R. The coefficients identification is performed from it and the difference to the true, not noisy, dense reference is evaluated using the ENL metric. The task is performed on 50 trials for each tested noise floor. The results are shown in Fig. 8. It shows that the truncation order T, depending on the noise floor R and the proposed number of samples, 1.25T, gives the expected reconstruction accuracy. The number of samples went from 356 for a noise floor of $R = -30$ dB to 660 for -70 dB.

D. Experimental Validation

The proposed small number of samples is applied to the characterization of two radiating structures of radically different shapes and operating frequencies measured in two different systems.

1) Standard gain horn at X band: The horn has been measured at 10 GHz in the MVG multi-probe system StarLab [32] of IETR-INSA, the measurement setup is shown in Fig.

This article has been accepted for publication in a future issue of this journal, but has not been fully edited. Content may change prior to final publication. Citation information: DOI 10.1109/TAP.2021.3118711, IEEE Transactions on Antennas and Propagation

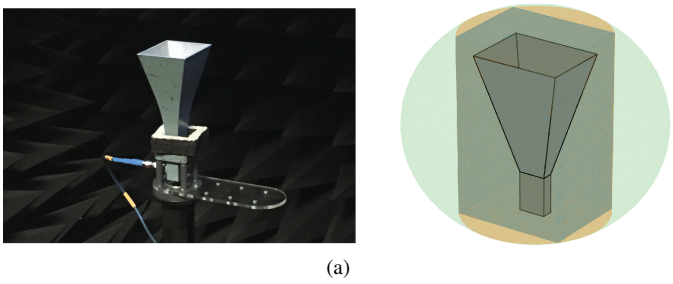

(a)

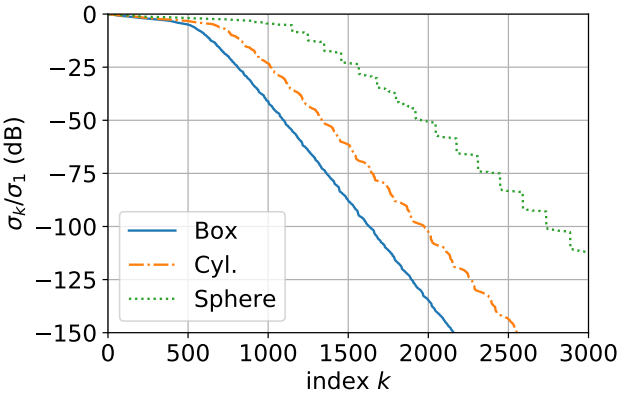

(b)

Fig. 9. (a) Photography of the horn and representation of the three equivalent current surfaces Σ (sphere, cylinder and box) used for the horn characterization. (b) Normalized singular value distribution of the corresponding radiation matrices.

9(a). The reference and data sets are generated in the far field at any position using the spherical coefficients returned by the MVG's software. Three equivalent current surfaces Σ enclosing the horn are considered : a box, a cylinder and a sphere, as shown in Fig. 9(a). The corresponding singular values of the radiation matrices are shown in Fig. 9(b). The considered minimal sphere has a radius a of 10 cm $\approx 3.3\lambda$. The measurement noise floor is estimated to be equal to $R = -45$ dB. As shown by the singular value distributions, the orders of the model T for the box, the cylinder and the sphere are $1141, 1389$ and 1966 respectively.

The validity of the proposed small number of samples (15) is shown in Fig. 10. The ENL metric between the reference field $\mathbf{y}$ and the one estimated from M_S samples is plotted for the three equivalent current surfaces as a function of M_S. First, the vertical lines, computed from (15), indicate when the aimed reconstruction accuracy should be achieved, ENL $\leq R = -45$ dB. Second, the surface that best fits the AUT (the box in this case) is clearly the one leading to the smallest number of samples.

The reconstructions of the far field over a cutting plane are shown in Fig. 11 in order to further demonstrate the importance of the choice of the surface surrounding the AUT. The small number of field samples advocated for the box, which better fits the geometry of the antenna, has been chosen, $M_S = 1448 \approx 1.25 \times 1141$. An excellent agreement between the reference and the reconstruction using the box is achieved whereas the two other surface shapes lead to inaccurate electric far fields.

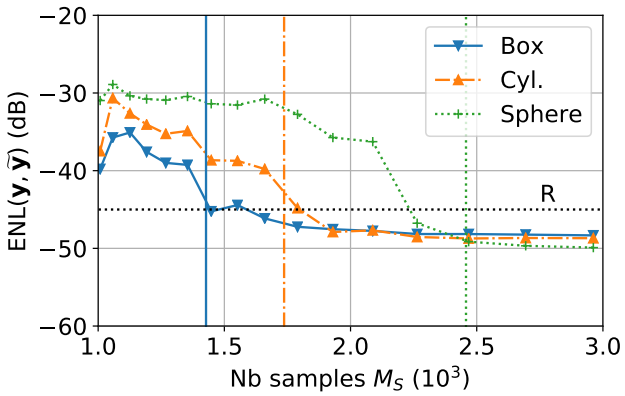

Fig. 10. ENL reconstruction metric between the reference field $\mathbf{y}$ and its estimation $\widetilde{\mathbf{y}}$ using the reduced order model for a noise floor of $R = -45$ dB for various sample sizes M_S. The vertical lines are the number of samples corresponding to an oversampling of $\chi = 1.25$ for the respective shapes.

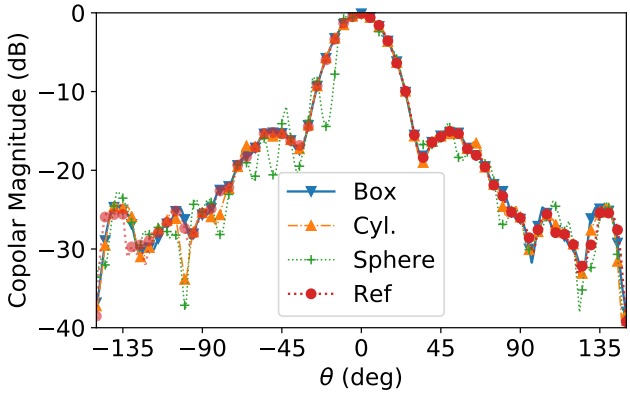

Fig. 11. Normalized copolar component of the X band horn at 10 GHz. The reference pattern is generated by the MVG software and other are reconstructed from only $M_s = 1448$ field samples, as advocated for the surface of the box (blue vertical line of Fig. 10). A proper reconstruction from the cylinder and sphere surfaces would require more field samples.

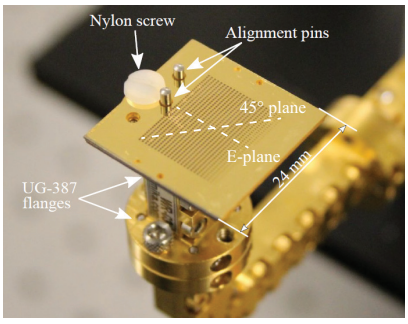

Fig. 12. Picture of the pillbox antenna designed by KTH and IETR [33]. The operating bandwidth spans from 220 to 300 GHz.

This article has been accepted for publication in a future issue of this journal, but has not been fully edited. Content may change prior to final publication. Citation information: DOI 10.1109/TAP.2021.3118711, IEEE Transactions on Antennas and Propagation

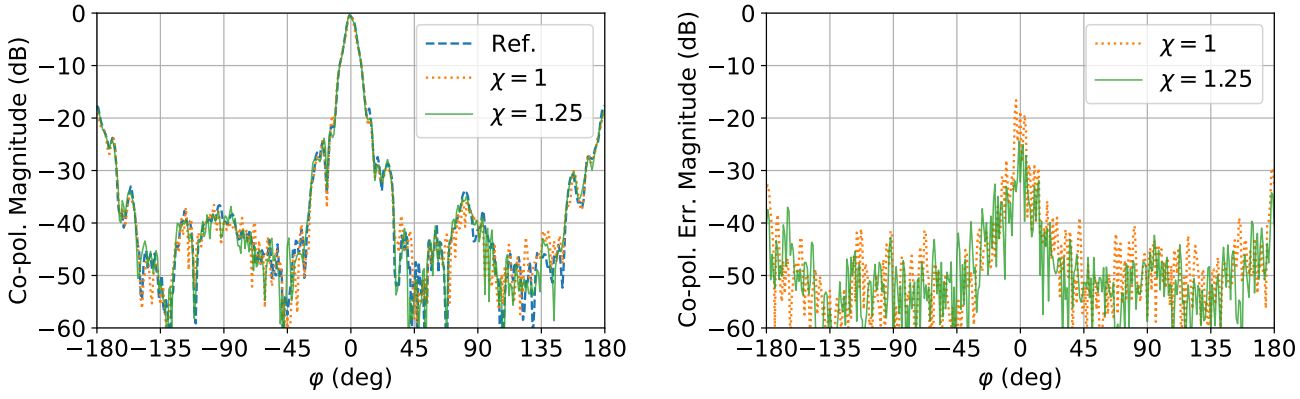

(a) (b)

Fig. 13. (a) Normalized reconstruction of the field co-polarization in the main cutting plane for different oversampling factors. (b) Absolute error on the reconstruction with respect to the reference.

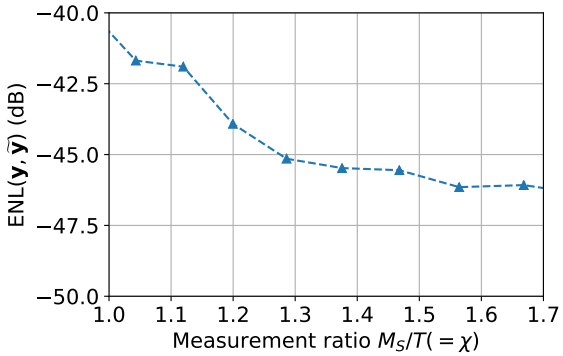

Fig. 14. ENL reconstruction metric between the reference field and its estimation using the reduced order model as a function of the measurement ratio (or oversampling factor).

2) Pillbox antenna at 230 GHz*:* Let us consider the pillbox antenna designed by KTH and IETR [33] measured in the far field at 230 GHz in the M^{2}ARS facilities at IETR, an image of the prototype is shown in Fig. 12. The measurement system [34] is a roll-over-azimuth positioning system performing step-by-step acquisition. The reference far-field pattern is provided by a densely measured field sampling and SW expansion. The considered equivalent surface is a box of dimensions $25\times25\times4$ mm, i.e. approximately $20\lambda\times20\lambda\times3\lambda$. A noise floor of $R=-45$ dB is assumed, leading to T $\approx 4.3\times10^3$ coefficients.

The ENL metric between the reference field and the reconstruction using the reduced-order model as a function of the measurement sampling M_S/T ratios, or equivalently of the oversampling factor χ, is shown in Fig. 14. An oversampling factor $\chi = 1.25$ is close to the optimal number of samples to reach the aimed accuracy, which confirms experimentally our previous studies. To provide an illustration of these results, the reconstruction of the field co-polarization in the main cutting plane and the error curve with respect to the reference are displayed in Fig. 13 for two oversampling factors χ.

E. Summary

The characterization of far-field patterns from a reduced number of samples has been experimentally validated using two very different antenna types, shapes and operating frequencies that have been characterized in two measurement systems; an all-in-one commercial system [32] and an academic laboratory anechoic chamber.

Less field samples are required when the convex surface surrounding the AUT is tailored to its shape, which confirms the link between the number of field samples and the area of the enclosing surface. Moreover, an oversampling value of $\chi = 1.25$ is shown to be a reasonable choice to find a small number of samples as confirmed by these experimental results.

V. Conclusion

The steps to determine a reduced number of samples to characterize the antenna far-field radiation pattern have been detailed. The proposed methodology calls for the construction of the radiation matrix involved in the antenna characterization problem. By appropriately truncating its singular value decomposition, a small dictionary of the possible far-fields radiated by the antenna under test is built for a chosen accuracy level. Instead of using all-purpose analytical basis functions exhibiting intrinsic symmetries, the proposed strategy enables to generate numerically a compressed basis tailored to the antenna being characterized. The practical relevance of the so-customized basis has been thoroughly investigated. The influence of the field sampling strategy, its robustness with respect to noise and equivalent current surface shape surrounding the antenna under test leads to a realistic small number of field samples. It is determined by the area of the surface enclosing the antenna under test. This work confirms, and somehow extends by means of numerical tools, the fundamental and pioneering analytical derivations on the minimum non-redundant sampling by Bucci *et al.* [10]. The proposed method has been applied to characterize the far field of two antennas at 10 and 230 GHz, respectively. These measurements, carried out in two different facilities, validate experimentally the proposed approach and show its potentialities. The extension of this work to the near-field characterization of antennas, where sampling strategies depend on the measurement surfaces, is under investigation.

ACKNOWLEDGMENT

The authors would like to thank Laurent Le Coq and Jérôme Sol for their help in measuring the antennas and many fruitful discussions. We also thank Athanasios G. Polimeridis for his insights on the reduced-order model approach.

REFERENCES

[1] M. Migliore, "Near field antenna measurement sampling strategies: From linear to nonlinear interpolation," *Electronics*, vol. 7, p. 257, 10 2018.

[2] J. Hald, J. Hansen, F. Jensen, and F. Larsen, *Spherical Near Field Antenna Measurements*, J. Hansen, Ed. Peter Peregrinus, 1988.

[3] O. M. Bucci and G. Franceschetti, "On the spatial bandwidth of scattered fields," *IEEE Trans. Antennas Propag.*, vol. 35, no. 12, pp. 1445–1455, 1989.

[4] R. Cornelius, D. Heberling, N. Koep, A. Behboodi, and R. Mathar, "Compressed sensing applied to spherical near-field to far-field transformation." Davos: Eur. Conf. Antennas Propag. (EuCAP), 2016.

[5] D. Loschenbrand and C. Mecklenbräuker, "Fast antenna characterization via a sparse spherical multipole expansion." Aachen: 4th International Workshop on Compressed Sensing Theory and its Applications to Radar, Sonar and Remote, 2016.

[6] B. Fuchs, L. Le Coq, S. Rondineau, and M. Migliore, "Fast antenna far field characterization via sparse spherical harmonic expansion," *IEEE Trans. Antennas Propag.*, vol. 65, no. 10, pp. 5503–5510, Oct. 2017.

[7] B. Hofmann, O. Neitz, and T. Eibert, "On the minimum number of samples for sparse recovery in spherical antenna near-field measurements," *IEEE Trans. on Antennas and Propag.*, July 2019.

[8] O. M. Bucci and G. Franceschetti, "On the degrees of freedom of scattered fields," *IEEE Trans. Antennas Propag.*, vol. 37, no. 7, pp. 918–926, 1989.

[9] O. M. Bucci, C. Gennarelli, and C. Savarese, "Optimal interpolation of radiated fields over a sphere," *IEEE Trans. Antennas Propag.*, vol. 39, no. 11, pp. 1633–1643, 1991.

[10] O. M. Bucci, C. Gennarelli, and C. Savarese, "Representation of electromagnetic fields over arbitrary surfaces by a finite and nonredundant number of samples," *IEEE Trans. Antennas Propag.*, vol. 46, no. 3, pp. 351–359, March 1998.

[11] G. Giordanengo, M. Righero, F. Vipiana, M. Sabbadini, and G. Vecchi, "Fast antenna testing with reduced near field sampling," *IEEE Trans. Antennas Propag.*, vol. 62, no. 5, pp. 2501–2513, May 2014.

[12] M. A. Saporetti, F. Saccardi, L. J. Foged, J. Zackrisson, M. Righero, G. Giordanengo, G. Vecchi, and D. Trenta, "Reduced sampling in nf antenna measurement using numerical defined expansion functions," in *2019 13th European Conference on Antennas and Propagation (EuCAP)*, 2019, pp. 1–4.

[13] M. Salucci, M. D. Migliore, G. Oliveri, and A. Massa, "Antenna measurements-by-design for antenna qualification," *IEEE Trans. on Antennas and Propag.*, vol. 66, no. 11, pp. 6300–6312, Nov 2018.

[14] Y. Alvarez, T. K. Sarkar, and F. Las-Heras, "Improvement of the sources reconstruction techniques: analysis of the svd algorithm and the rwg basis functions," in *2007 IEEE Antennas and Propagation Society International Symposium*, 2007, pp. 5644–5647.

[15] T. B. Hansen, A. Paulus, and T. F. Eibert, "On the condition number of a normal matrix in near-field to far-field transformations," *IEEE Transactions on Antennas and Propagation*, vol. 67, no. 3, pp. 2028–2033, 2019.

[16] L. Matekovits, V. A. Laza, and G. Vecchi, "Analysis of large complex structures with the synthetic-functions approach," *IEEE Transactions on Antennas and Propagation*, vol. 55, no. 9, pp. 2509–2521, 2007.

[17] B. Stupfel and Y. Morel, "Singular value decomposition of the radiation operator—application to model-order and far-field reduction," *IEEE Trans. Antennas Propag.*, vol. 56, no. 6, pp. 1605–1615, June 2008.

[18] B. Fuchs and A. Polimeridis, "Reduced-order models for fast antenna characterization," *IEEE Trans. Antennas Propag.*, vol. 67, no. 8, pp. 5673–5677, Aug. 2019.

[19] R. F. Harrington, *Time-Harmonic Electromagnetic Fields*. IEEE-Press, 2001.

[20] J. L. Araque Quijano, L. Scialacqua, J. Zackrisson, L. J. Foged, M. Sabbadini, and G. Vecchi, "Suppression of undesired radiated fields based on equivalent currents reconstruction from measured data," *IEEE Antennas and Wireless Propagation Letters*, vol. 10, pp. 314–317, 2011.

[21] J. L. Araque Quijano and G. Vecchi, "Improved-accuracy source reconstruction on arbitrary 3-d surfaces," *IEEE Antennas and Wireless Propagation Letters*, vol. 8, pp. 1046–1049, 2009.

[22] ——, "Field and source equivalence in source reconstruction on 3d surfaces," *Progress In Electromagnetics Research*, vol. 103, pp. 67 – 100, 2010.

[23] J. Kornprobst, R. Mauermayer, O. Neitz, J. Knapp, and T. Eibert, "On the solution of inverse equivalent surface-source problems," *Progress In Electromagnetics Research*, vol. 165, pp. 47–65, 01 2019.

[24] S. Rao, D. Wilton, and A. Glisson, "Electromagnetic scattering by surfaces of arbitrary shape," *IEEE Trans. Antennas Propag.*, vol. 30, no. 3, pp. 409–418, 1982.

[25] M. Abramowitz and I. A. Stegun, *Handbook of Mathematical Functions with Formulas, Graphs, and Mathematical Tables*. New York: Dover, 1964.

[26] P. Hansen, "The L-curve and its use in the numerical treatment of inverse problems," in *Computational Inverse Problems in Electrocardiology*. WIT Press, 2000.

[27] F. Jensen and A. Frandsen, "On the number of modes in spherical wave expansions," in *AMTA Proceedings*, 2004.

[28] W. Chew, E. Michielssen, J. M. Song, and J. M. Jin, *Fast and Efficient Algorithms in Computational Electromagnetics*. USA: Artech House, Inc., 2001.

[29] F. D'Agostino, F. Ferrara, J. A. Fordham, C. Gennarelli, R. Guerriero, and M. Migliozzi, "An experimental validation of the near-field - far-field transformation with spherical spiral scan [amta corner]," *IEEE Antennas and Propagation Magazine*, vol. 55, no. 3, pp. 228–235, 2013.

[30] F. D'Agostino, F. Ferrara, C. Gennarelli, R. Guerriero, and M. Migliozzi, "Far-field reconstruction from near-field data acquired via a fast spherical spiral scan: Experimental evidences," *Progress In Electromagnetics Research*, vol. 140, pp. 719–732, 2013.

[31] C. A. Balanis, *Antenna Theory: Analysis and Design*. Wiley-Interscience, 2005.

[32] MVG. Starlab 650 MHz-18 GHz. [Online]. Available: https://www.mvg-world.com/fr/products/antenna-measurement/multi-probe-systems/starlab

[33] A. Gomez-Torrent, M. Garcia-Vigueras, L. Le Coq, A. Mahmoud, M. Ettorre, R. Sauleau, and J. Oberhammer, "A low-profile and high-gain frequency beam steering subterahertz antenna enabled by silicon micromachining," *IEEE Trans. Antennas Propag.*, vol. 68, no. 2, pp. 672–682, Aug. 2020.

[34] "Plateforme M2ARS," IETR-UR1, 2020, available at https://www.ietr.fr/plateforme-m2ars-manufacturing-measurement-analysis-radiating-systems.